

Self-Supervised Learning for Detecting AI-Generated Faces as Anomalies

Mian Zou

City University of Hong Kong
Hong Kong, Hong Kong
mianzou2-c@my.cityu.edu.hk

Baosheng Yu

Nanyang Technological University
Singapore
baosheng.yu@ntu.edu.sg

Yibing Zhan

JD Explore Academy
Beijing, China
zhanyibing@jd.com

Kede Ma[✉]

City University of Hong Kong
Hong Kong, Hong Kong
kede.ma@cityu.edu.hk

Abstract—The detection of AI-generated faces is commonly approached as a binary classification task. Nevertheless, the resulting detectors frequently struggle to adapt to novel AI face generators, which evolve rapidly. In this paper, we describe an anomaly detection method for AI-generated faces by leveraging self-supervised learning of camera-intrinsic and face-specific features purely from photographic face images. The success of our method lies in designing a pretext task that trains a feature extractor to rank four ordinal exchangeable image file format (EXIF) tags and classify artificially manipulated face images. Subsequently, we model the learned feature distribution of photographic face images using a Gaussian mixture model. Faces with low likelihoods are flagged as AI-generated. Both quantitative and qualitative experiments validate the effectiveness of our method. Our code is available at https://github.com/MZMMSEC/AIGFD_EXIF.git.

Index Terms—AI-generated face detection, anomaly detection, self-supervised learning.

I. INTRODUCTION

AI-generated faces, produced using techniques such as generative adversarial networks (GANs) [1], [2] and diffusion models [3]–[8], have become nearly indistinguishable from those captured by digital cameras [9]. This raises concerns about their potential misuse, making their detection crucial for countering misinformation, preserving multimedia integrity, and ensuring trust in sensitive visual data.

Traditional methods for detecting AI-generated faces typically rely on binary classification, in which detectors are trained to differentiate between photographic and AI-generated images [10]–[20]. However, such methods often lack generalizability to newly emerging AI face generators with distinct design philosophies, higher-quality training data, and better optimization pipelines. As a result, existing detectors that are overly tuned to specific generative models may quickly become obsolete when faced with unfamiliar generators.

To address this generalization challenge, an alternative strategy treats AI-generated face images as anomalies within the distribution of photographic face images, a concept known as anomaly detection or one-class classification in machine learning [21]. Successful implementations of this strategy include exploiting physiological cues like pupil shapes [22], head poses [23], and corneal specular highlights [24] to expose physical and/or biological irregularities. However, hand-engineered features might have limited utility against

photorealistic AI-generated faces. Recently, Ojha *et al.* [25] demonstrated the potential of pre-trained CLIP features [26] for detecting AI-generated images, though CLIP’s semantic focus may not be optimal for media forensics.

In this study, we advance the anomaly detection of AI-generated faces through self-supervised representation learning. Inspired by prior work on exchangeable image file format (EXIF) data for image splicing detection [27], [28], we design a pretext task that involves ranking [29] four ordinal, EXIF tags (*i.e.*, aperture, exposure time, focal length, and ISO speed) and classifying artificially manipulated face images. Optimized using an equally weighted sum of fidelity losses across these five subtasks [30], [31], the learned camera-intrinsic and face-specific features enable anomaly detection of AI-generated faces through a Gaussian mixture model (GMM) [32]. Extensive experiments on nine state-of-the-art generative models [1]–[8] confirm the effectiveness of our method in detecting AI-generated faces.

II. PROPOSED METHOD

In this section, we present in detail the construction of our anomaly detection method for AI-generated faces, including self-supervised representation learning and GMM training. The system diagram is presented in Fig. 1.

A. Self-Supervised Representation Learning

We design an image feature extractor $\mathbf{f}(\cdot; \boldsymbol{\theta}) : \mathbb{R}^{H \times W \times 3} \mapsto \mathbb{R}^N$, parameterized by $\boldsymbol{\theta}$, which computes the visual embedding $\mathbf{f}(\mathbf{x})$ for a given face image $\mathbf{x} \in \mathbb{R}^{H \times W \times 3}$. Here, H and W denote the image height and width, respectively. Additionally, we employ five prediction heads $g(\cdot; \boldsymbol{\phi}_i) : \mathbb{R}^N \mapsto \mathbb{R}$, for $i \in \{1, \dots, 5\}$, collectively parameterized by $\boldsymbol{\phi}$. These heads are used to compute the “logits” for four EXIF tag ranking tasks and one face manipulation classification task.

EXIF Tag Ranking. Given a photographic face image pair (\mathbf{x}, \mathbf{y}) , we first derive a binary ground-truth label for the i -th EXIF tag:

$$p_i(\mathbf{x}, \mathbf{y}) = \begin{cases} 1 & \text{if } \text{tag}_i(\mathbf{x}) \geq \text{tag}_i(\mathbf{y}), \text{ for } i \in \{1, \dots, 4\}, \\ 0 & \text{otherwise} \end{cases}, \quad (1)$$

where $\text{tag}_i(\cdot)$ outputs the recorded value of the i -th tag from the pre-selected EXIF set: {aperture, exposure

[✉]Corresponding author.

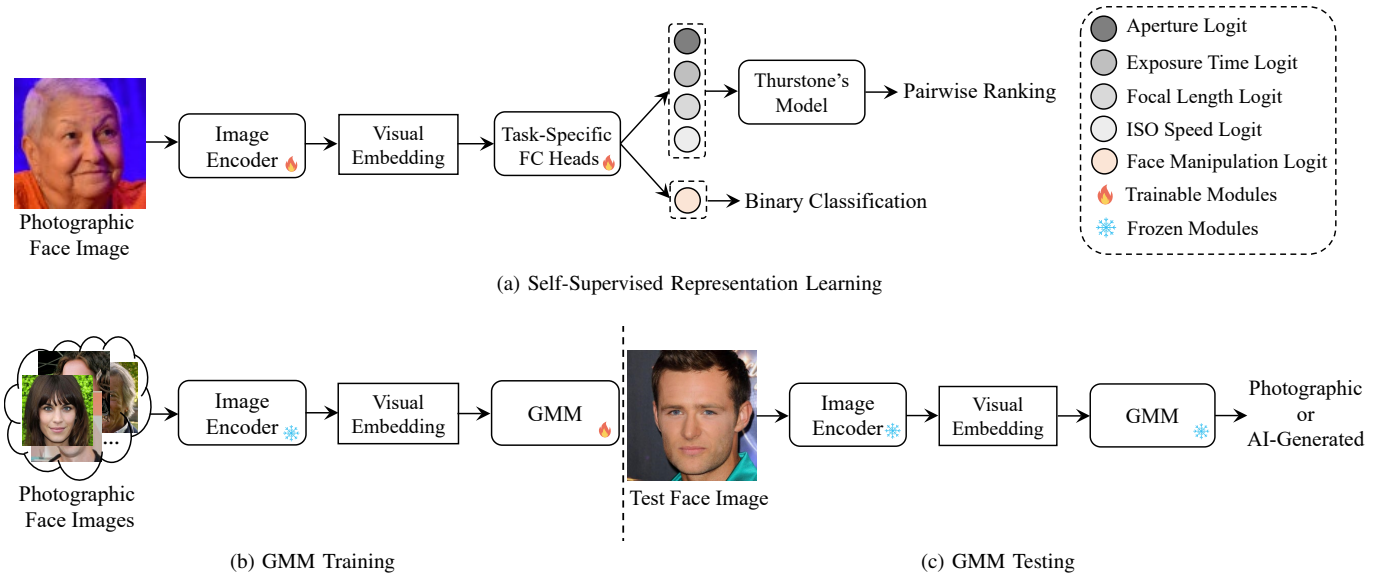


Fig. 1. System diagram of the construction of the proposed anomaly detection method for AI-generated faces, including self-supervised representation learning and GMM training. During testing, faces with low likelihoods are identified as AI-generated.

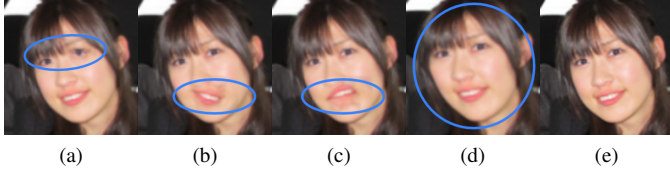


Fig. 2. Visual examples of artificially manipulated face images by (a) horizontal eye flipping, (b) horizontal mouth flipping, (c) vertical mouth flipping, and (d) global affine transformation, respectively. (e) The original face is also shown as the reference.

time, focal length, ISO speed}. Under the Thurstone’s model [33], we estimate the probability that the i -th EXIF tag of \mathbf{x} is larger than that of \mathbf{y} as

$$\hat{p}(\mathbf{x}, \mathbf{y}; \theta, \phi_i) = \Phi \left(\frac{g(\mathbf{f}(\mathbf{x}; \theta); \phi_i) - g(\mathbf{f}(\mathbf{y}; \theta); \phi_i)}{\sqrt{2}} \right), \quad (2)$$

where $\Phi(\cdot)$ is the standard normal cumulative distribution function. We then adopt the fidelity loss [30] for the EXIF tag ranking task:

$$\ell(\mathbf{x}, \mathbf{y}; \theta, \phi_i) = 1 - \sqrt{p_i(\mathbf{x}, \mathbf{y})\hat{p}(\mathbf{x}, \mathbf{y}; \theta, \phi_i)} - \sqrt{(1 - p_i(\mathbf{x}, \mathbf{y}))(1 - \hat{p}(\mathbf{x}, \mathbf{y}; \theta, \phi_i))}. \quad (3)$$

Face Manipulation Classification. We introduce artificial manipulations to photographic face images via 1) horizontal eye flipping, 2) horizontal mouth flipping, 3) vertical mouth flipping, and 4) global affine transformation, as shown in Fig. 2. The process of local face part flipping is outlined in Fig. 3. Specifically, for a given photographic face image as input, we first detect its 68 face landmarks [34] to define a region-of-interest mask. The identified local face part, according to the mask, is then flipped and linearly blended into the original face image. For global affine transformation, we utilize the `PiecewiseAffine` API function from the publicly available toolbox—`imgaug` [35].

For consistency, we also employ the fidelity loss for the face manipulation classification task:

$$\ell(\mathbf{x}; \theta, \phi_5) = 1 - \sqrt{p(\mathbf{x})\hat{p}(\mathbf{x}; \theta, \phi_5)} - \sqrt{(1 - p(\mathbf{x}))(1 - \hat{p}(\mathbf{x}; \theta, \phi_5))}, \quad (4)$$

where $p(\mathbf{x}) = 1$ indicates that \mathbf{x} has been manipulated and

$$\hat{p}(\mathbf{x}; \theta, \phi_5) = \text{Sigmoid}(g(\mathbf{f}(\mathbf{x}; \theta); \phi_5)) \quad (5)$$

is the corresponding estimated probability.

Overall Loss. Given a training minibatch $\mathcal{B}_{\text{tr}} = \{\mathbf{x}^{(m)}\}_{m=1}^M$, we form all possible image pairs and derive the corresponding binary labels using Eq. (1), which are collectively denoted as \mathcal{P}_{tr} . Then, the overall loss can be computed by

$$\ell(\mathcal{B}_{\text{tr}}; \theta, \phi) = \frac{1}{|\mathcal{P}_{\text{tr}}|} \sum_{(\mathbf{x}, \mathbf{y}) \in \mathcal{P}_{\text{tr}}} \sum_{i=1}^4 \ell(\mathbf{x}, \mathbf{y}; \theta, \phi_i) + \frac{1}{|\mathcal{B}_{\text{tr}}|} \sum_{\mathbf{x} \in \mathcal{B}_{\text{tr}}} \ell(\mathbf{x}; \theta, \phi_5). \quad (6)$$

B. GMM Training and Testing

We approach AI-generated face detection as an anomaly detection problem. To achieve this, we build the probability distribution of the learned features of photographic face images using a GMM with K components:

$$p(\mathbf{z}) = \sum_{k=1}^K \pi_k \mathcal{N}(\mathbf{z}; \boldsymbol{\mu}_k, \boldsymbol{\Sigma}_k), \quad (7)$$

where $\mathbf{z} = \mathbf{f}(\mathbf{x})$ represents the feature vector of \mathbf{x} . π_k is the k -th mixing coefficient with the constraint that $\sum_{k=1}^K \pi_k = 1$, and $\boldsymbol{\mu}_k$ and $\boldsymbol{\Sigma}_k$ are the mean and covariance of the k -th Gaussian component. We use the expectation-maximization algorithm for GMM parameter estimation.

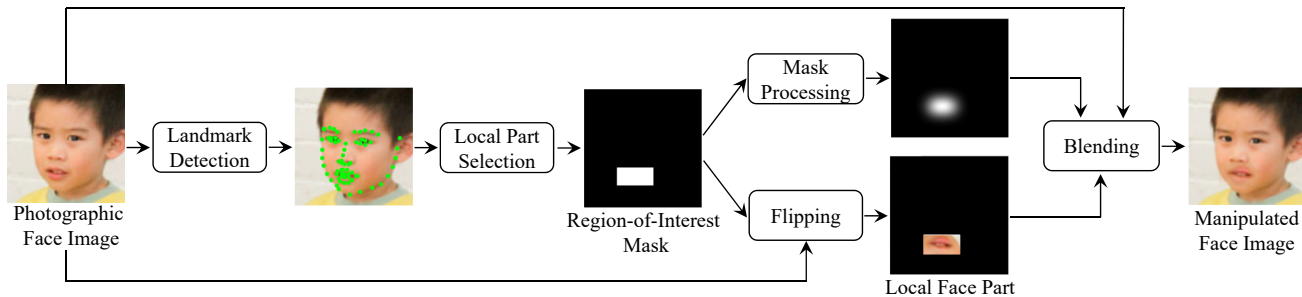


Fig. 3. The process of local face part flipping as a form of artificial face manipulation.

TABLE I

MAIN RESULTS OF OUR METHOD AGAINST SIX REPRESENTATIVE AI-GENERATED FACE DETECTORS IN TERMS OF ACC AND AP. THE BEST RESULTS ARE HIGHLIGHTED IN BOLD, WHILE THE SECOND-BEST RESULTS ARE UNDERLINED

Method	StyleGAN2		VQGAN		LDM		DDIM		SDv2.1		FreeDoM		HPS		Midjourney		SDXL		Average	
	Acc	AP	Acc	AP	Acc	AP	Acc	AP	Acc	AP	Acc	AP	Acc	AP	Acc	AP	Acc	AP	Acc	AP
GramNet [12]	51.16	78.74	99.92	100.00	53.25	80.15	50.09	58.59	50.23	52.90	51.59	76.77	50.26	48.28	52.91	63.52	53.63	65.45	57.00	69.38
FRDM [18]	70.13	99.93	100.00	100.00	99.62	100.00	98.26	100.00	62.48	83.41	55.68	98.28	75.07	96.69	92.51	99.56	89.77	99.19	82.61	97.45
RECCE [41]	66.64	76.10	100.00	100.00	70.91	81.69	73.10	81.15	71.62	80.71	77.52	82.80	64.14	96.40	62.19	96.28	65.29	95.67	72.38	87.87
LGrad [39]	52.94	91.54	99.99	100.00	99.80	100.00	64.91	98.28	57.59	93.78	66.58	49.16	60.14	96.04	76.59	98.69	74.03	98.30	72.43	91.75
DIRE [15]	72.48	90.34	69.81	89.82	98.92	100.00	77.80	91.80	58.84	74.16	<u>89.05</u>	94.26	62.50	78.30	90.75	97.43	87.79	96.46	78.66	90.29
UnivFD [25]	65.45	71.47	83.40	97.58	70.06	76.61	72.25	81.02	72.76	80.66	78.55	86.88	56.21	60.10	54.96	56.35	58.01	60.76	67.96	74.60
Ours	76.88	83.94	74.59	82.85	93.83	<u>98.67</u>	<u>93.63</u>	<u>98.67</u>	78.62	87.60	95.31	99.86	83.79	91.15	<u>91.29</u>	97.32	91.71	97.38	86.63	93.01

During testing, we calculate the log-likelihoods of test image features, flagging those with low likelihoods as AI-generated.

III. EXPERIMENTS

A. Experimental Setups

Datasets. We gather 200,000 face photos, each with four EXIF tags—aperture, exposure time, focal length, and ISO speed—from FDF [36] for self-supervised representation learning. Following [12], [16], [37]–[39], we use 25,000 face images from the CelebA-HQ dataset [40] to build the GMM, with additional 5,000 images reserved for testing. Meanwhile, we collect AI-generated face images from nine state-of-the-art models, including StyleGAN2 [1], VQGAN [2], LDM [3], DDIM [4], Stable Diffusion 2.1 (SDv2.1) [3], FreeDoM [5], HPS [6], Midjourney [7], and SDXL [8]. These images are either sourced from public datasets [37], [38] or generated on demand [1], [2].

Implementation Details. Our method utilizes ResNet-50 [42] as the backbone for feature extraction, resulting in a feature dimension N of 768. We use the initializations from [28] and set the input image size to $224 \times 224 \times 3$. During self-supervised representation learning, we minimize the objective in Eq. (6) using Adam [43] with a decoupled weight decay of 10^{-4} and a minibatch size of 256, for a total of 20 epochs. The initial learning rate is set to 10^{-5} , which follows a cosine annealing schedule [44]. The number of Gaussian components K in the GMM is set to eight.

Evaluation Metrics. We adopt the detection accuracy (Acc (%)) and average precision (AP (%)) as the evaluation metrics. We set a low-likelihood threshold that gives a 5% false alarm rate (*i.e.*, the 5-th percentile) in the training set to screen

TABLE II

AUC RESULTS OF GMM-BASED DETECTORS USING DIFFERENT PRE-TRAINED FEATURES. EXIF-L2R IS A DEGENERATE OF OUR METHOD THAT ONLY LEARNS TO RANK THE FOUR EXIF TAGS

Generator	CLIP	FaRL	EXIF-LAN	EXIF-L2R	Ours
StyleGAN2	33.99	34.35	69.71	67.91	85.69
VQGAN	60.20	55.91	72.41	69.99	84.31
LDM	55.49	47.26	85.81	83.20	98.66
DDIM	82.85	85.10	84.98	87.94	97.96
SDv2.1	90.15	95.24	74.21	86.74	88.29
FreeDom	85.39	79.91	97.92	93.84	99.79
HPS	91.22	93.97	87.33	90.30	91.92
Midjourney	92.21	89.72	91.65	94.06	97.07
SDXL	93.66	94.61	93.04	95.39	97.23
Average	76.13	75.12	84.12	85.49	93.43

AI-generated faces. Additionally, we employ the area under the curve (AUC (%)) to assess the discriminative power of pre-trained features.

B. Main Results

In line with prior studies [25], [45], [46], our experiments focus on evaluating generalizability. We compare our method with six representative detectors: GramNet [12], FRDM [18], RECCE [41], LGrad [39], UnivFD [25], and DIRE [15]. For a fair comparison, we retrain all competing methods on the same datasets (*i.e.*, CelebA-HQ and VQGAN-generated images), adhering strictly to the training protocols and hyperparameter settings described in the original publications. The only exception is DIRE, which is trained on the CelebA-HQ and LDM datasets, as it relies on reconstruction errors of diffusion models. Table I shows the main results, from which we have

TABLE III
ABLATION ON THE PRETEXT TASK FOR SELF-SUPERVISED
REPRESENTATION LEARNING

EXIF Tag Ranking	Face Manipulation Classification	Mean Acc	Mean AP
✓	✗	69.35	86.44
✗	✓	77.67	84.23
✓	✓	86.63	93.01

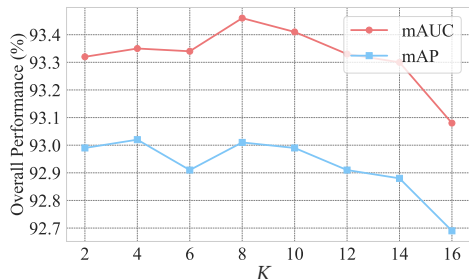


Fig. 4. Ablation on the number of Gaussian components of the GMM.

some key observations. First, despite being trained exclusively on photographic face images, our method archives the highest average accuracy, surpassing the second-best detector by a substantial margin of 4.02%. Notably, our method successfully detects AI-generated faces by commercial APIs such as Midjourney [7] and SDv2.1 [3]. Second, UnivFD, which utilizes semantic CLIP features [26], exhibits marginal performance, indicating that semantics of photographic and AI-generated faces become increasingly indistinguishable, consistent with the findings in [9]. Third, frequency-based (*i.e.*, FRDM [18]) and gradient-based (*i.e.*, LGrad [39]) methods, trained on GAN-based images, also perform well on diffusion-based images in terms of AP, suggesting a shared presence of low-level artifacts as detection cues. However, their relatively lower accuracies point to potential overfitting issues. Finally, DIRE [15] encounters challenges in generalizing to the same family of diffusion models, emphasizing the significant impact of the evolution of generative models on detection accuracy.

C. Comparisons with Other Pre-Trained Features

We compare our proposed self-supervised features against four alternatives by 1) CLIP [26], 2) FaRL [47], 3) EXIF-as-language (EXIF-LAN) [28], and 4) a degenerate of our method that only learns to rank the four EXIF tags (EXIF-L2R), within the same GMM framework. CLIP is pre-trained contrastively on massive image-text pairs to capture high-level image semantics, while FaRL and EXIF-LAN can be seen as variants of CLIP. FaRL is pre-trained solely on face images, and EXIF-LAN aligns images with corresponding EXIF tags. As shown in Table II, our features outperform all counterparts, validating the usefulness of the proposed self-supervised learning method in improving feature discriminability. In contrast, semantics-oriented features (*i.e.*, by CLIP and FaRL) fall short in detecting AI-generated faces. In addition, the superiority of EXIF-L2R

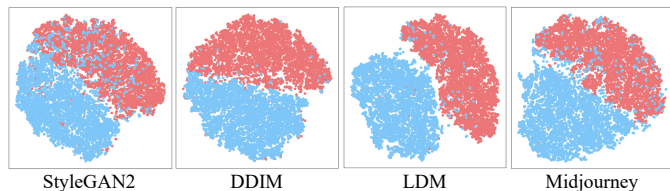


Fig. 5. t-SNE embeddings [48] of self-supervised features for photographic (in red) and AI-generated (in blue) face images.

over EXIF-LAN verifies the importance of capturing more fine-grained ordinal information of EXIF tags in learning EXIF-induced features.

D. Further Analysis

Ablation Studies. We first analyze two degenerates of our pretext task: 1) minimizing only Eq. (3) and 2) minimizing only Eq. (4) in self-supervised representation learning. From the results in Table III, it is clear that the full pretext task results in the best performance, thereby confirming its design rationale. Next, we tune the number of Gaussian components (*i.e.*, K in Eq. (7)) on a separate validate set to see its variability in detection performance. Fig. 4 shows fairly stable performance across different values of K , with the best results at $K = 8$.

Visualizations. Fig. 5 illustrates 2D embeddings of pre-trained features for photographic and AI-generated faces using t-SNE [48], highlighting a clear separation between the two classes. This further validates the effectiveness of our self-supervised representation learning method in capturing unique characteristics of photographic face images.

IV. CONCLUSION AND DISCUSSION

We have introduced an AI-generated face detector based on self-supervised anomaly detection. Central to our method is the design of a pretext task that encourages learning camera intrinsic and face-specific features from photographic face images. Experimental results demonstrate the promise of our self-supervised features in detecting AI-generated faces.

The present study is limited to detecting AI-generated faces. Future work could expand the proposed idea to detect a broader range of AI-generated content. Moreover, exploring the joint optimization of self-supervised representation learning and anomaly detection, potentially in a bilevel framework [49], could be a promising direction. Additionally, leveraging self-supervised features as guidance [50], [51] could potentially improve the training of a binary classifier for AI-generated faces [12], [15], [18], [39], [52].

ACKNOWLEDGEMENTS

This work was supported in part by the Hong Kong RGC General Research Fund (11220224), the CityU Strategic Research Grants (7005848 and 7005983), and an Industry Gift Fund (9229179).

REFERENCES

- [1] T. Karras, S. Laine, M. Aittala, J. Hellsten, J. Lehtinen, and T. Aila, "Analyzing and improving the image quality of StyleGAN," in *CVPR*, 2020, pp. 8110–8119.
- [2] P. Esser, R. Rombach, and B. Ommer, "Taming Transformers for high-resolution image synthesis," in *CVPR*, 2021, pp. 12873–12883.
- [3] R. Rombach, A. Blattmann, D. Lorenz, P. Esser, and B. Ommer, "High-resolution image synthesis with latent diffusion models," in *CVPR*, 2022, pp. 10684–10695.
- [4] J. Song, C. Meng, and S. Ermon, "Denoising diffusion implicit models," in *ICLR*, 2021, pp. 1–20.
- [5] J. Yu, Y. Wang, C. Zhao, B. Ghanem, and J. Zhang, "FreeDoM: Training-free energy-guided conditional diffusion model," in *ICCV*, 2023, pp. 23174–23184.
- [6] K. Lee, H. Liu, M. Ryu, O. Watkins, Y. Du, C. Boutilier, P. Abbeel, M. Ghavamzadeh, and S. S. Gu, "Aligning text-to-image models using human feedback," in *ICCV*, 2023, pp. 2096–2015.
- [7] "Midjourney," <https://www.midjourney.com>, Accessed: Aug 11, 2024.
- [8] D. Podell, Z. English, K. Lacey, A. Blattmann, T. Dockhorn, J. Müller, J. Penna, and R. Rombach, "SDXL: Improving latent diffusion models for high-resolution image synthesis," in *ICLR*, 2024, pp. 1–13.
- [9] S. J. Nightingale and H. Farid, "AI-synthesized faces are indistinguishable from real faces and more trustworthy," *PNAS*, vol. 119, no. 8, pp. 1–3, 2022.
- [10] M. K. Johnson and H. Farid, "Exposing digital forgeries through chromatic aberration," in *ACM MM&Sec*, 2006, pp. 48–55.
- [11] F. Matern, C. Riess, and M. Stamminger, "Exploiting visual artifacts to expose deepfakes and face manipulations," in *WACVW*, 2019, pp. 83–92.
- [12] Z. Liu, X. Qi, and P. H. Torr, "Global texture enhancement for fake face detection in the wild," in *CVPR*, 2020, pp. 8060–8069.
- [13] Ning Yu, Larry S Davis, and Mario Fritz, "Attributing fake images to GANs: Learning and analyzing GAN fingerprints," in *ICCV*, 2019, pp. 7556–7566.
- [14] D. Gragnaniello, D. Cozzolino, F. Marra, G. Poggi, and L. Verdoliva, "Are GAN generated images easy to detect? A critical analysis of the state-of-the-art," in *ICME*, 2021, pp. 1–6.
- [15] Z. Wang, J. Bao, W. Zhou, W. Wang, H. Hu, H. Chen, and H. Li, "DIRE for diffusion-generated image detection," in *ICCV*, 2023, pp. 22445–22455.
- [16] R. Durall, M. Keuper, and J. Keuper, "Watch your up-convolution: CNN based generative deep neural networks are failing to reproduce spectral distributions," in *CVPR*, 2020, pp. 7890–7899.
- [17] R. Corvi, D. Cozzolino, G. Poggi, K. Nagano, and L. Verdoliva, "Intriguing properties of synthetic images: from generative adversarial networks to diffusion models," in *CVPRW*, 2023, pp. 973–982.
- [18] Y. Luo, Y. Zhang, J. Yan, and W. Liu, "Generalizing face forgery detection with high-frequency features," in *CVPR*, 2021, pp. 16317–16326.
- [19] C. Dong, A. Kumar, and E. Liu, "Think twice before detecting GAN-generated fake images from their spectral domain imprints," in *CVPR*, 2022, pp. 7865–7874.
- [20] J. Frank, T. Eisenhofer, L. Schönherr, A. Fischer, D. Kolossa, and T. Holz, "Leveraging frequency analysis for deep fake image recognition," in *ICML*, 2020, pp. 3247–3258.
- [21] D. M. Hawkins, *Identification of Outliers*, Springer, 1980.
- [22] H. Guo, S. Hu, X. Wang, M.-C. Chang, and S. Lyu, "Eyes tell all: Irregular pupil shapes reveal GAN-generated faces," in *ICASSP*, 2022, pp. 2904–2908.
- [23] X. Yang, Y. Li, and S. Lyu, "Exposing Deep Fakes using inconsistent head poses," in *ICASSP*, 2019, pp. 8261–8265.
- [24] S. Hu, Y. Li, and S. Lyu, "Exposing GAN-generated faces using inconsistent corneal specular highlights," in *ICASSP*, 2021, pp. 2500–2504.
- [25] U. Ojha, Y. Li, and Y. J. Lee, "Towards universal fake image detectors that generalize across generative models," in *CVPR*, 2023, pp. 24480–24489.
- [26] A. Radford, J. W. Kim, C. Hallacy, A. Ramesh, G. Goh, S. Agarwal, G. Sastry, A. Askell, P. Mishkin, J. Clark, G. Krueger, and I. Sutskever, "Learning transferable visual models from natural language supervision," in *ICML*, 2021, pp. 8748–8763.
- [27] M. Huh, A. Liu, A. Owens, and A. A. Efros, "Fighting fake news: Image splice detection via learned self-consistency," in *ECCV*, 2018, pp. 101–117.
- [28] C. Zheng, A. Shrivastava, and A. Owens, "EXIF as language: Learning cross-modal associations between images and camera metadata," in *CVPR*, 2023, pp. 6945–6956.
- [29] C. Burges, T. Shaked, E. Renshaw, A. Lazier, M. Deeds, N. Hamilton, and G. Hullender, "Learning to rank using gradient descent," in *ICML*, 2005, pp. 89–96.
- [30] M.-F. Tsai, T.-Y. Liu, T. Qin, H.-H. Chen, and W.-Y. Ma, "FRank: A ranking method with fidelity loss," in *ACM SIGIR*, 2007, pp. 383–390.
- [31] M. Zou, B. Yu, Y. Zhan, S. Lyu, and K. Ma, "Semantics-oriented multitask learning for DeepFake detection: A joint embedding approach," *arXiv preprint arXiv:2408.16305*, 2024.
- [32] G. J. McLachlan and K. E. Basford, *Mixture Models: Inference and Applications to Clustering*, Marcel Dekker, 1988.
- [33] L. L. Thurstone, "A law of comparative judgment," *Psychol. Rev.*, vol. 34, pp. 273–286, Jul. 1927.
- [34] A. Bulat and G. Tzimiropoulos, "How far are we from solving the 2D & 3D face alignment problem? (and a dataset of 230,000 3D facial landmarks)," in *ICCV*, 2017, pp. 1021–1030.
- [35] "Imgaug," <https://imgaug.readthedocs.io/en/latest/source/overview/geometric.html>, Accessed: Aug 11, 2024.
- [36] H. Hukkelås, R. Mester, and F. Lindseth, "DeepPrivacy: A generative adversarial network for face anonymization," in *ISVC*, 2019, pp. 565–578.
- [37] H. Cheng, Y. Guo, T. Wang, L. Nie, and M. Kankanhalli, "Diffusion facial forgery detection," *arXiv preprint arXiv:2401.15859*, 2024.
- [38] Z. Chen, K. Sun, Z. Zhou, X. Lin, X. Sun, L. Cao, and R. Ji, "DiffusionFace: Towards a comprehensive dataset for diffusion-based face forgery analysis," *arXiv preprint arXiv:2403.18471*, 2024.
- [39] C. Tan, Y. Zhao, S. Wei, G. Gu, and Y. Wei, "Learning on gradients: Generalized artifacts representation for GAN-generated images detection," in *CVPR*, 2023, pp. 12105–12114.
- [40] T. Karras, T. Aila, S. Laine, and J. Lehtinen, "Progressive growing of GANs for improved quality, stability, and variation," in *ICLR*, 2018, pp. 1–26.
- [41] J. Cao, C. Ma, T. Yao, S. Chen, S. Ding, and X. Yang, "End-to-end reconstruction-classification learning for face forgery detection," in *CVPR*, 2022, pp. 4113–4122.
- [42] K. He, X. Zhang, S. Ren, and J. Sun, "Deep residual learning for image recognition," in *CVPR*, 2016, pp. 770–778.
- [43] D. P. Kingma and J. Ba, "Adam: A method for stochastic optimization," in *ICLR*, 2015, pp. 1–15.
- [44] I. Loshchilov and F. Hutter, "SGDR: Stochastic gradient descent with warm restarts," in *ICLR*, 2017, pp. 1–13.
- [45] D. Cozzolino, G. Poggi, M. Nießner, and L. Verdoliva, "Zero-shot detection of AI-generated images," in *ECCV*, 2024, pp. 54–72.
- [46] Riccardo Corvi, Davide Cozzolino, Giada Zingarini, Giovanni Poggi, Koki Nagano, and Luisa Verdoliva, "On the detection of synthetic images generated by diffusion models," in *ICASSP*, 2023, pp. 1–5.
- [47] Y. Zheng, H. Yang, T. Zhang, J. Bao, D. Chen, Y. Huang, L. Yuan, D. Chen, M. Zeng, and F. Wen, "General facial representation learning in a visual-linguistic manner," in *CVPR*, 2022, pp. 18697–18709.
- [48] L. van der Maaten and G. Hinton, "Visualizing data using t-SNE," *JMLR*, vol. 9, no. 86, pp. 2579–2605, 2008.
- [49] Stephan Dempe, *Foundations of Bilevel Programming*, Springer Science & Business Media, 2002.
- [50] Z. Li and D. Hoiem, "Learning without forgetting," *IEEE TPAMI*, vol. 40, no. 12, pp. 2935–2947, 2017.
- [51] A. Haliassos, R. Mira, S. Petridis, and M. Pantic, "Leveraging real talking faces via self-supervision for robust forgery detection," in *CVPR*, 2022, pp. 14950–14962.
- [52] S.-Y. Wang, O. Wang, R. Zhang, A. Owens, and A. A. Efros, "CNN-generated images are surprisingly easy to spot...for now," in *CVPR*, 2020, pp. 8695–8704.